Low Temperature Physics/Fizika Nizkikh Temperatur, 2017, v. 43, No. 12, pp. 1761–1772

Phonon excitations in the quasi-one-dimensional Haldane phase of $SrNi_2V_2O_8$

V. Kurnosov[1], V. Gnezdilov[1, 2], P. Lemmens[2], Yu. Pashkevich[3], A.K. Bera[4], A.T.M.N. Islam[4], and B. Lake[4]

[1]*B. Verkin Institute for Low Temperature Physics and Engineering, NASU, Kharkov 61103, Ukraine*

[2]*Institute for Condensed Matter Physics, TU Braunschweig, D-38106 Braunschweig, Germany*

[3]*A.A. Galkin Donetsk Institute for Physics and Engineering, NASU, Kyiv 03680, Ukraine*

[4]*Helmholtz-Zentrum Berlin, Hahn-Meitner-Platz 1, Berlin 14109, Germany*

E-mail: kurnosov@ilt.kharkov.ua

Received April 4, 2017, published online October 25, 2017

Vibrational Raman spectra of a single crystal of the coupled Haldane chain compound $SrNi_2V_2O_8$ with uniaxial anisotropy were investigated in the 10–1000 cm^{-1} frequency range at temperatures 7–300 K. No structural phase transition was observed. The number of phonon lines observed in the experiment and their intensity were analyzed on the basis of the local symmetry considerations of different structural complexes. This approach was successful in explaining the discrepancy between the numbers of expected and experimentally observed phonon lines. Closeness of a real arrangement of some structural units to higher symmetry than the Wyckoff position results in strong interferential quenching of a number of Raman lines in the spectra.

PACS: **78.30.–j** Infrared and Raman spectra;
63.20.–e Phonons in crystal lattices.

Keywords: Raman intensity, local symmetry consideration, interferential quenching.

1. Introduction

A remarkable feature of one-dimensional (1D) magnetic systems is the suppression of long-range magnetic order even at zero temperature by strong quantum spin fluctuations. Spin-1 Heisenberg antiferromagnetic (AFM) chains (Haldane chains) are of current interest due to their exotic magnetic properties [1,2]. The Haldane phase of integer spin chains has a unique many-body singlet ground state and gapped magnetic excitations [3,4] in contrast to the gapless continuum of multispinon excitations of its half-integer counterpart, the spin-1/2 Heisenberg uniform AFM chain. The magnetic excitation spectra of an isolated Haldane chain were investigated in great detail using theoretical methods [5–7], as well as experimental techniques [8,9].

Raman scattering was proven to be a versatile tool to investigate compounds that represent low-dimensional quantum spin systems [10]. In addition to spin excitations, also excitations of the lattice system or even coupled modes can be investigated. This may help to better understand the effect of the lattice degrees of freedom on the spin system. Despite the great interest in Haldane chains materials, there are very few studies of these systems using Raman spectroscopy. To our present knowledge, detailed investigations only exist for the one $S = 1$ spin chain compound Y_2BaNiO_5 [11].

In real systems the presence of interchain interactions and anisotropy leads to complex behaviors and a rich phase diagram as theoretically described in Ref. 12. In this regard compounds $ANi_2V_2O_8$, where A = Sr or Pb, are of interest since they have substantial interchain interactions and single-ion uniaxial anisotropy [13,14]. According to earlier experiments on powder samples [13,15] the ground state of $SrNi_2V_2O_8$ was suggested to be 3D ordered below ~7 K. Later, in numerous experiments [16–22] it has been convincingly shown that $SrNi_2V_2O_8$ has a nonmagnetic spin-singlet ground state.

Our present research activities aim to analyze phonon excitations of the quasi-1D Haldane compound $SrNi_2V_2O_8$ in detail. These are based on the study of the crystal symmetry and phonon excitations that in many cases help to uncover fundamental properties.

2. Experimental

Details of the $SrNi_2V_2O_8$ single crystals growth and characterization can be found in Refs. 19, 20. Our Raman scatter-

ing experiments were performed in a quasi-backscattering geometry on *ab* and *ac* surfaces of $SrNi_2V_2O_8$ single crystals. A solid-state laser with the excitation wavelengths $\lambda = 532.1$ nm and a power level $P = 5$ mW was used for the spectra excitation. Spectra of the scattered radiation were collected by a Dilor-XY triple spectrometer and recorded by a liquid-nitrogen-cooled CCD detector (Horiba Jobin Yvon, Spectrum One CCD-3000V) with a spectral resolution of <0.5 cm^{-1}. In our experiments we used parallel (*aa, cc*) and crossed (*ab, ac*) light polarizations. Temperature dependences of the Raman spectra were measured in a variable temperature closed cycle cryostat (Oxford/Cryomech Optistat, RT-2.8 K).

3. Phonon spectra

3.1. Group theoretical analysis and polarization rules

The structure of $SrNi_2V_2O_8$ is described by the space group $I4_1cd$ (#110, C_{4v}^{12}) with $z = 8$ formula units per unit cell [20,23]. According our knowledge, there is no evidence of structural instabilities for temperatures below room temperature. Due to the existence of the "rigid" ionic complexes $(VO_4)^{3-}$ the vibrational modes may be expressed formally in terms of internal and external degrees of freedom of these extended complexes and with respect to degrees of freedom of the point ions Sr^{2+} and Ni^{2+} (see Table 1).

Table 1. Representation of $SrNi_2V_2O_8$ vibrational modes in terms of internal and external degrees of freedom of ionic complexes $(VO_4)^{3-}$ and translations of point ions Sr^{2+} and Ni^{2+} using the space group $I4_1cd$ and 8 formula units per unit cell

Ions, modes		Irreps
Sr^{2+}, translational		$1A_1+1A_2+1B_1+1B_2+4E$
Ni^{2+}, translational		$3A_1+3A_2+3B_1+3B_2+6E$
$(VO_4)^{3-}$, translational		$3A_1+3A_2+3B_1+3B_2+6E$
$(VO_4)^{3-}$, rotational		$3A_1+3A_2+3B_1+3B_2+6E$
Lattice optical		$9A_1+10A_2+10B_1+10B_2+21E$
Lattice acoustic		A_1+E
$(VO_4)^{3-}$, internal	ν_1 (A_1)	$1A_1+1A_2+1B_1+1B_2+2E$
	ν_2 (E)	$2A_1+2A_2+2B_1+2B_2+4E$
	ν_3 (F_2)	$3A_1+3A_2+3B_1+3B_2+6E$
	ν_4 (F_2)	$3A_1+3A_2+3B_1+3B_2+6E$
$(VO_4)^{3-}$, internal (total)		$9A_1+9A_2+9B_1+9B_2+18E$

There are 4 Raman-active irreps A_1, B_1, B_2, and E whose polarizability tensors in coordinates corresponding to crystallographic directions of 4*mm* (C_{4v}) have the form

$$A_1, z \to \begin{pmatrix} a & & \\ & a & \\ & & b \end{pmatrix}, B_1 \to \begin{pmatrix} & c & \\ c & & \\ & & \end{pmatrix}, B_2 \to \begin{pmatrix} & & d \\ & & \\ d & & \end{pmatrix},$$

$$E, x \to \begin{pmatrix} & & e \\ & & \\ e & & \end{pmatrix}, E, y \to \begin{pmatrix} & & \\ & & e \\ & e & \end{pmatrix}. \qquad (1)$$

If orientations of *x* and *y* axes are not precisely determined, the above matrices, excluding fully symmetrical irrep A_1, may be generally rewritten as

$$B_1(\theta) \to \begin{pmatrix} c\cos 2\theta & c\sin 2\theta & \\ c\sin 2\theta & -c\cos 2\theta & \\ & & \end{pmatrix},$$

$$B_2(\theta) \to \begin{pmatrix} -d\sin 2\theta & d\cos 2\theta & \\ d\cos 2\theta & d\sin 2\theta & \\ & & \end{pmatrix}, \qquad (2)$$

$$E, x(\theta) \to \begin{pmatrix} & & e\cos\theta \\ & & e\sin\theta \\ e\cos\theta & e\sin\theta & \end{pmatrix},$$

$$E, y(\theta) \to \begin{pmatrix} & & -e\sin\theta \\ & & e\cos\theta \\ -e\sin\theta & e\cos\theta & \end{pmatrix},$$

where θ is an angle between real crystallographic direction and arbitrary direction in the basal plane of the crystal. According to (2) the uncertainty in the orientation leads to a mixing of the polarization selection rules for Raman lines which belong to phonons with B_1 and B_2 symmetry. On the one hand, such mixing makes B_1 and B_2 modes unresolved, but, on the other hand, it helps to resolve A_1 and B_1 (and/or B_2) ones. Polarization *zz* is "pure" for A_1 modes, all other are forbidden. It seems that this property is useful for the identification of A_1 type modes and their selection in other polarizations. But here we face some peculiarity: the polar character of the A_1 modes leads to a splitting of their longitudinal (LO) and transversal (TO) components.

In opaque crystals the observation of LO and TO components of polar phonons in Raman spectra depends on specifics of experimental back scattering geometry. This information is collected in Table 2.

Experimental Raman data were obtained using two sample orientations so that plane of incident light reflection contained c_4 axis of the crystal, or was perpendicular to it. Table 2 shows, for instance, that in *zz* polarization only A_1 modes are present (and only TO components), while in $x'x'$ polarization, besides B_1 and B_2 phonons, A_1 modes are present (LO components). So, for A_1 modes possessing large LO–TO splitting *zz* and $x'x'$ polarized spectra are different in the positions of the lines.

3.2. Structure of the Raman spectrum and molecular vibrations of $(VO_4)^{3-}$

The free ion $(VO_4)^{3-}$ is a tetrahedral complex and described within the T_d point group. It possesses 9 internal degrees of freedom, which are grouped into 4 modes transformed as $A_1(\nu_1)+E(\nu_2)+2F_2(\nu_3+\nu_4)$ irreps of T_d. Two of them belong to so-called symmetric $A_1(\nu_1)$ and asymmetric $F_2(\nu_3)$ stretchings of V–O valence bonds. They have a priori the highest vibrational frequency. Two remaining

Table 2. Raman selection rules for phonons of a different symmetry in the quasi-back scattering geometry utilized in the experiments. Symbols: **q** is direction of phonon wave-vector, $\mathbf{e}_i$ and $\mathbf{e}_s$ are polarizations of an incident and scattered light, respectively, $\alpha = \cos\theta$, $\beta = \sin\theta$. Intensities of a scattering are evaluated using the tensor components from (1)

q	$\mathbf{e}_i$	$\mathbf{e}_s$	A_1	E	B_1	B_2
(0,0,1)	(α,β,0)	(α,β,0)	a^2 (LO)		$(\alpha^2-\beta^2)^2c^2$	$4(\alpha\beta)^2d^2$
(0,0,1)	(α,β,0)	(β,–α,0)			$4(\alpha\beta)^2c^2$	$(\alpha^2-\beta^2)^2d^2$
(α,β,0)	(0,0,1)	(0,0,1)	b^2 (TO)			
(α,β,0)	(β,–α,0)	(0,0,1)		e^2 (TO)		

vibrational modes of the (VO_4) tetrahedron are the symmetric $E(\nu_2)$ and asymmetric $F_2(\nu_4)$ bendings of the valence angles. Their frequencies are very close in the free complex and are more than twice less than the frequency of stretching mode ν_1. In crystals the characteristic frequency ranges of these modes are: $A_1(\nu_1)$ — 800–900, $E(\nu_2)$ — 300–450, $F_2(\nu_3)$ — 700–900, $F_2(\nu_4)$ — 300–450 см$^{-1}$ [24–30]. In aqueous solutions of $(VO_4)^{3-}$ containing salts the frequencies are: $A_1(\nu_1)$ — 826±1, $F_2(\nu_3)$ — (804±4) см$^{-1}$, $E(\nu_2)$ and $F_2(\nu_4)$ — (336±2) см$^{-1}$ [31].

The O^{2-} ion has a large enough ionic radius of ~1.38 Å [32], so oxides structures often may be described like a lattice of these close packed ions, voids between which are occupied by "small" metallic ions. $SrNi_2V_2O_8$ has quite such structure, where the octahedral surrounding of every Ni^{2+} ion consists of the same O^{2-} ions that belong to six different $(VO_4)^{3-}$ complexes. Octahedral oxygen complexes of transitional metals are very popular units representing metal-oxide crystal structures too. The internal vibrations of (NiO_6) octahedrons reach frequencies of about 550 cm^{-1} [33–35], so the individuality of all internal modes of $(VO_4)^{3-}$ tetrahedra becomes doubtful. Looking on the Raman spectra of $SrNi_2V_2O_8$ one can divide them into two ranges: 50–500 and 700–950 cm^{-1} (Fig. 1). It is clear that the high-frequency region is occupied by vibrations that originate from $A_1(\nu_1)$ and $F_2(\nu_3)$ internal modes of 8 $(VO_4)^{3-}$ tetrahedra contained in the primitive cell. Only these modes keep their individuality and are well isolated from the low-frequency "lattice" vibration region. In contrast the bending modes of $(VO_4)^{3-}$ tetrahedra merge with other modes of the crystal, producing the so-called "lattice" region. According to the Table 1, high-frequency region of the $SrNi_2V_2O_8$ Raman spectrum must contain lines corresponding to $4A_1+4B_1+4B_2+8E$ irreps ($4A_2$ irreps are silent). The lattice range corresponds to $14A_1+15B_1+15B_2+31E$ Raman-active vibrational modes, accordingly.

Let us consider the spectral features of the high-frequency region: Spectra in all experimental polarizations at low temperature are presented in Fig. 2. The decomposition into the series of Lorentz-shape-like spectral lines is presented ibid. At low temperatures the most intensive A_1 lines show an appreciable asymmetry on the high-frequency slope. The high-temperature spectra don't reveal such features due to a temperature induced broadening of the lines. The nature of such asymmetry is not in the center of the present paper. As a suitable hypothesis we propose, that it may be a result of the combination of intensive optical modes with acoustical modes. Asymmetry in this case reflects a difference between the probabilities to excite and annihilate acoustic phonons, which is larger at low temperatures. High temperature equalizes the probabilities and makes the wings of the line symmetrical.

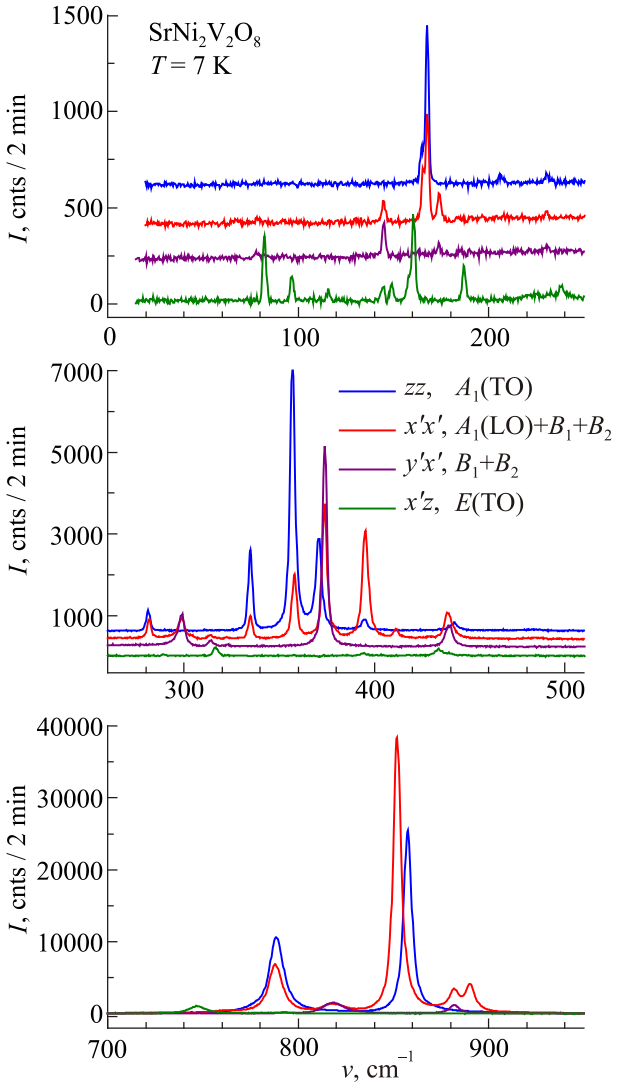

Fig. 1. (Color online) Raman spectra of $SrNi_2V_2O_8$ single crystal at $T = 7$ K in four polarizations. Irreps of Raman-active phonon excitations for every polarization are indicated.

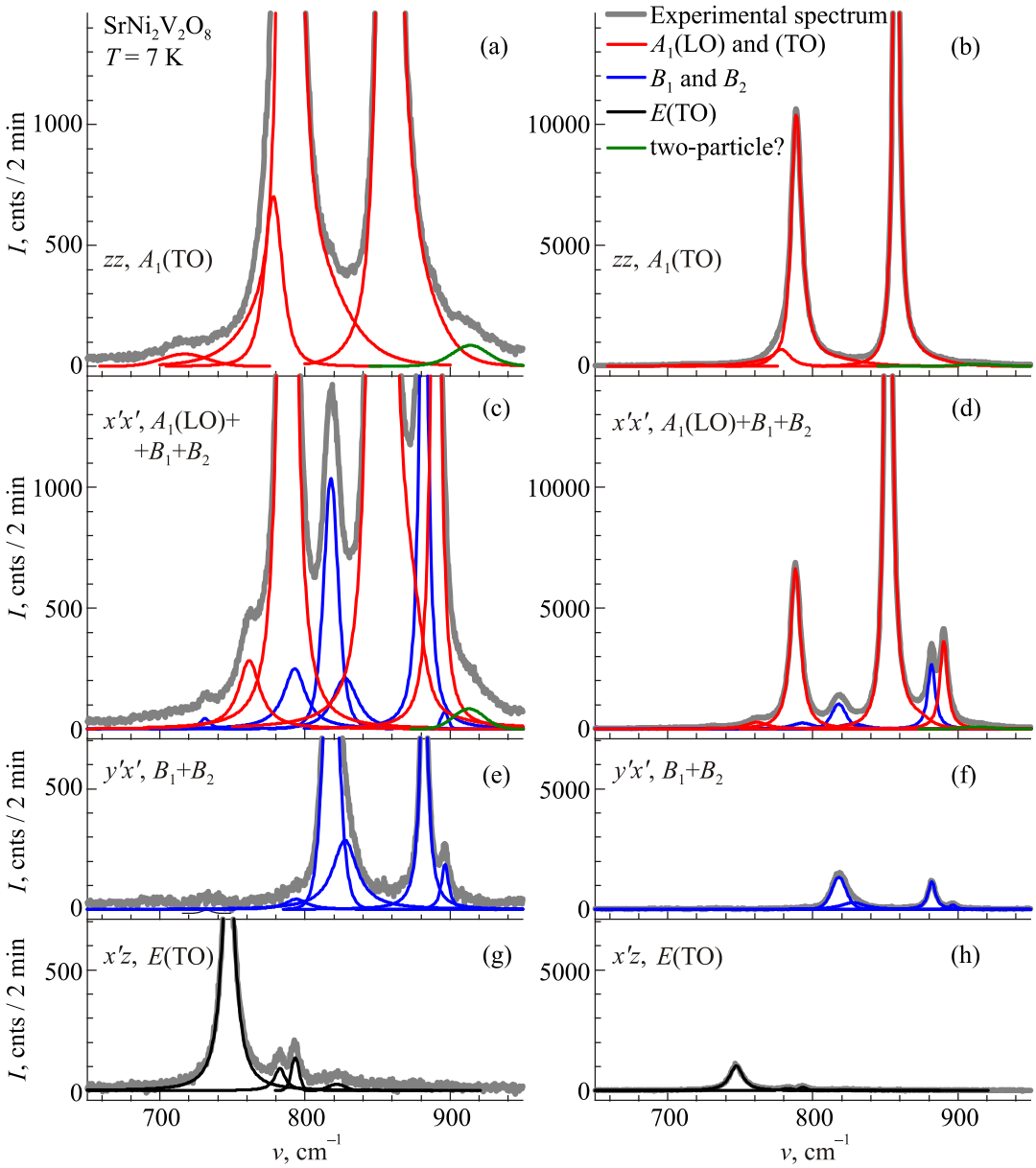

Fig. 2. (Color online) High-frequency Raman spectra of $SrNi_2V_2O_8$ in the range of $\nu_1(A_1)$ and $\nu_3(F_2)$ vibrational modes of $(VO_4)^{3-}$ complex. Polarization and corresponding symmetry of the modes are marked. Intensity scales on left and right panels differ in 10 times.

All identified lines are collected in Table 3. The spectrum in *zz* polarization with A_1(TO) consists of 5 lines, four of which are the Davydov components of $\nu_1(A_1)$ and $\nu_3(F_2)$ stretching modes of the $(VO_4)^{3-}$ tetrahedron (Fig. 2(a), (b)). Note, that triple degeneracy of $\nu_3(F_2)$ mode is lifted due to crystal field effect. The most intense line at 857.5 cm^{-1} must be attributed to the ν_1 mode according to frequency position. So, the highest-frequency line at 914 cm^{-1} most likely refers to some kind of two-particle excitation. The identical line is situated in $x'x'$ spectrum and has zero LO–TO splitting (Fig. 2(c), (d)). This spectrum contains a set of lines belonging to A_1(LO), B_1, and B_2 modes. *B* modes may be identified by means of a $y'x'$ polarized spectrum (Fig. 2(e), (f)). Remaining spectrum of $x'z$ polarization contains lines related to *E*(TO) modes.

The most intense line (ν_1) is observed in diagonal polarizations *zz* and $x'x'$. It demonstrates a so-called "inverted" LO–TO splitting (see Table 3). Originally, in the frame of T_d symmetry of a free $(VO_4)^{3-}$ complex, this mode is nonpolar. It is in agreement with a small observed LO–TO splitting. Inversion is a result of a fall of its energy into a wide, forbidden gap of some strong dipolar mode. The same "inversion", but with smaller splitting is inherent in the other intensive line (ν_3) at 788 cm^{-1}. Most probably the dipole mode with great oscillator strength originates from a polar ν_3 mode of a $(VO_4)^{3-}$ tetrahedron and possesses 778.2 (TO)–890.2 (LO) cm^{-1} splitting that covers the greater part of discussed spectral range. As was mentioned above, every internal degree of freedom, taking into account its degeneracy, produces 4 different one-dimensional irreps

Table 3. Frequencies, integral intensities and assignment of Raman lines observed in the spectral range of $\nu_1(A_1)$ and $\nu_3(F_2)$ vibrational modes of $(VO_4)^{3-}$ complex in $SrNi_2V_2O_8$

Frequency, cm^{-1}	Integral intensity, arb. units	Irreps	Polarization	Mode
717.0	1991	A_1(TO)	zz	
761.6	7832	A_1(LO)	$x'x'$	
731.5	451	B_1+B_2	$x'x'$	ν_3
	201	B_1+B_2	$y'x'$	
747.2	16606	E(TO)	$x'z$	
778.2	12734	A_1(TO)	zz	
890.2	33888	A_1(LO)	$x'x'$	
782.7	1271	E(TO)	$x'z$	ν_3
793.2	958	E(TO)	$x'z$	
793.4	7188	B_1+B_2	$x'x'$	
	1236	B_1+B_2	$y'x'$	
788.0	80697	A_1(LO)	$x'x'$	
788.4	138057	A_1(TO)	zz	
817.9	14509	B_1+B_2	$x'x'$	
	17922	B_1+B_2	$y'x'$	ν_3
821.7	387	E(TO)	$x'z$	
827.5	5594	B_1+B_2	$x'x'$	
	9116	B_1+B_2	$y'x'$	
851.9	282998	A_1(LO)	$x'x'$	
857.5	196273	A_1(TO)	zz	
881.9	24959	B_1+B_2	$x'x'$	
	11177	B_1+B_2	$y'x'$	ν_1
896.3	445	B_1+B_2	$x'x'$	
	1585	B_1+B_2	$y'x'$	
914.0	2902	A_1(TO)	zz	two-particle
912.9	2241	A_1(LO)	$x'x'$	

(A_1, A_2, B_1, B_2) and 2 two-dimensional ones (E) in the crystal. So, there are 4 groups of lines, each belongs to one degree of freedom, and must be presented by $A_1+B_1+B_2+2E$ symmetry. Figure 2 and Table 3 reveal detection of all 4 A_1 lines, 6 B_1+B_2 lines versus 8 allowed, and 4 E lines versus 8 allowed.

3.3. Low-frequency Raman spectra of $SrNi_2V_2O_8$

The low-frequency "lattice" range of Raman spectra does not show noticeable anomalies in their temperature dependence. Spectra in four polarizations belonging to phonons of different symmetry are presented in Fig. 3. The temperature dependences of the frequencies of all detected lines are shown in Fig. 4. A list of all detected phonon lines at lowest temperature with the indication of their symmetry and related polarization rules are given in Table 4. The total number of observed and detected low-temperature lines is essentially smaller than the group theory predicts. Only 11 from 14 A_1, 15 from 30 (B_1+B_2), and 16 from 31 E of allowed phononic lines are detected. The cause of such a deficit is probably the big number of formula units in the crystal unit cell that leads to small Raman intensities of some modes due to practically full interferential quenching. These aspects are considered in the following section.

4. Symmetry aspects of the phonon excitations intensity in the Raman spectrum of $SrNi_2V_2O_8$

Intensity of the Raman scattering originates from a polarizability induced by an appropriate mode in the crystal. Group theoretical analysis gives the total number of the modes based on the symmetry positions of the ions in the structure. Symmetry of some complexes (dimensions, angles, etc.) of a crystal structure sometimes appears higher than their Wyckoff positions. It may lead to the extremely weak intensity of some Raman signals. The following sections cover these issues.

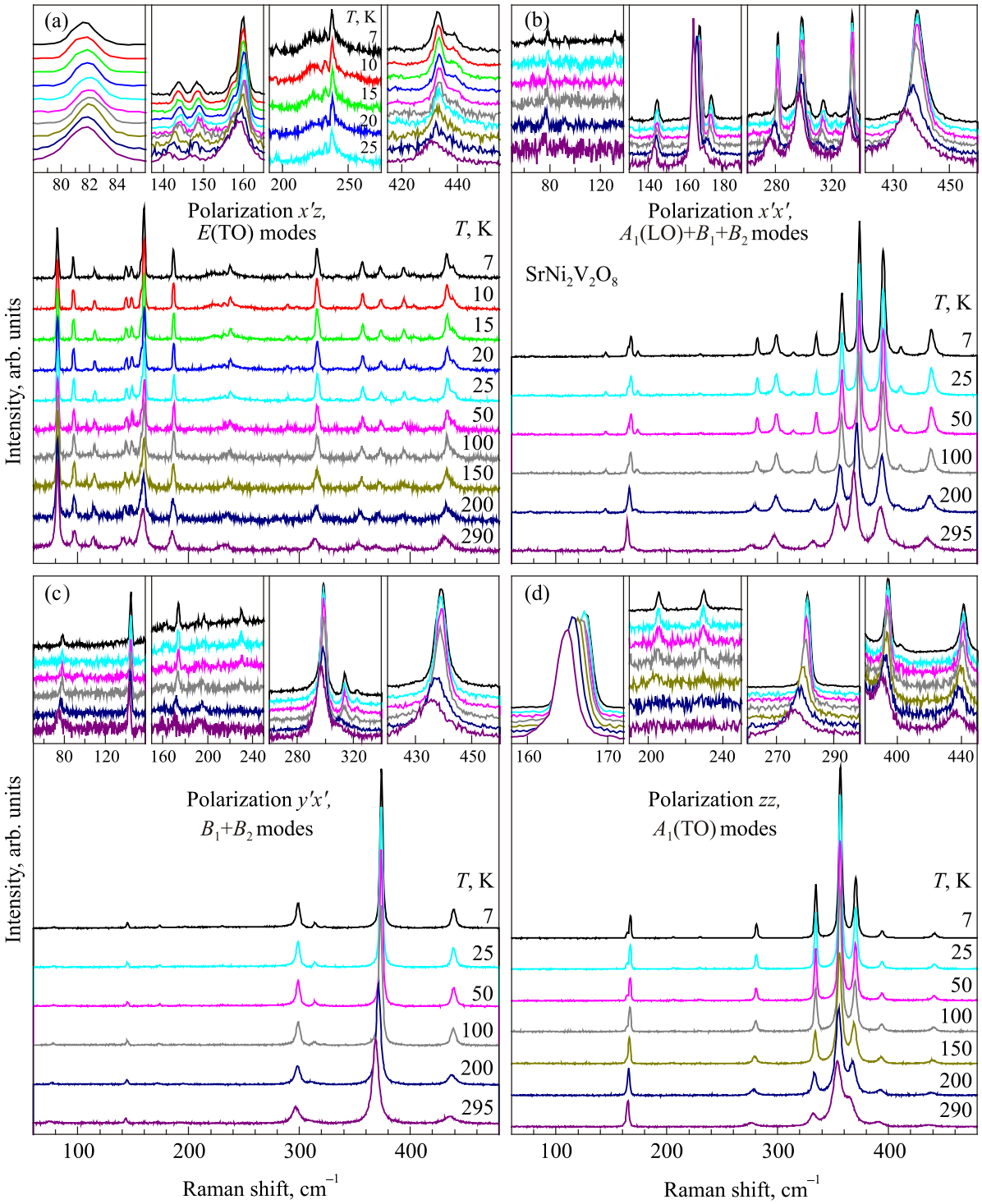

Fig. 3. (Color online) Temperature dependences of low-frequency range of $SrNi_2V_2O_8$ Raman spectrum in: (a) $x'z$ polarization corresponding to E(TO) modes, (b) $x'x'$ polarization corresponding to A_1(LO)+B_1+B_2 modes, (c) $y'x'$ polarization corresponding to B_1+B_2 modes, and (d) zz polarization corresponding to A_1(TO) modes. Insets show some spectral peculiarities in detail.

4.1. $(VO_4)^{3-}$ *modes*

In the structure of $SrNi_2V_2O_8$ the $(VO_4)^{3-}$ complexes occupy general positions, but their local second order axes in the T_d symmetry notation are oriented close to the principal axes of the crystal. More precisely, there are two groups of the tetrahedra whose second order axes are practically parallel to x and y crystallographic directions. Furthermore, the tetrahedra are slightly rotated around these preferred axes as can be seen in Fig. 5. We also consider some uniaxial distortion of the tetrahedra along those preferred axes in order to include to their polarizability some small parameters reflected the low symmetry of the position.

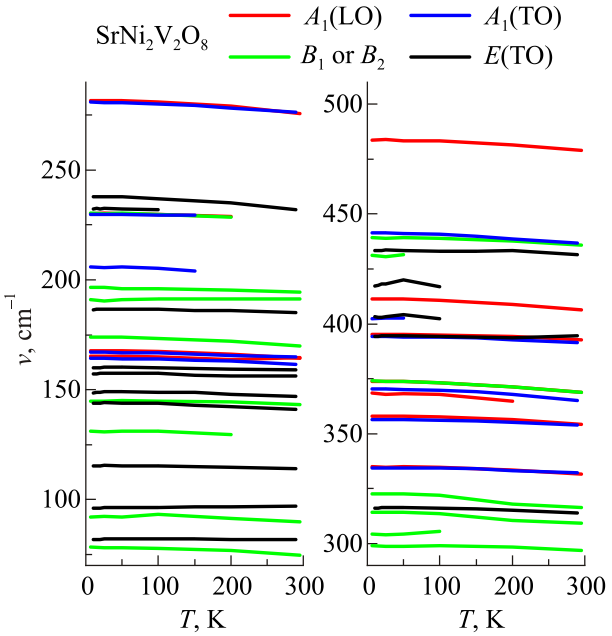

Fig. 4. (Color online) Temperature dependences of frequencies of all detected Raman-active phonons in the low-frequency range in $SrNi_2V_2O_8$.

Using such approach, the polarizabilities of an individual VO_4 tetrahedron related with its own modes in the crystal are expressed in the following manner:

$$\alpha_{\rm mol}^{A_1}(A_1)=\begin{pmatrix} a+\Delta_a & & \\ & a & \\ & & a \end{pmatrix},\quad \alpha_{\rm mol}^{A_1}(E(1))=\begin{pmatrix} -2b & & \\ & b & \\ & & b \end{pmatrix},$$

$$\alpha_{\rm mol}^{B_1}(E(2))=\begin{pmatrix} 0 & & \\ & \sqrt{3}b & \delta_b \\ & \delta_b & -\sqrt{3}b \end{pmatrix},\quad \alpha_{\rm mol}^{B_2(x)}(F_2(x))=\begin{pmatrix} & & \\ & \delta_c & c \\ & c & -\delta_c \end{pmatrix},$$

$$\alpha_{\rm mol}^{E(y)}(F_2(y))=\begin{pmatrix} & \delta_d & d \\ \delta_d & & \\ d & & \end{pmatrix},\quad \alpha_{\rm mol}^{E(z)}(F_2(z))=\begin{pmatrix} & d & -\delta_d \\ d & & \\ -\delta_d & & \end{pmatrix}, \tag{3}$$

where term Δ_a and difference between c and d are due to an uniaxial distortion of the tetrahedron along x axis; terms δ_b, δ_c, and δ_d are due to slight rotation around x axis. Using these assumptions and symmetry coordinates of nondegenerated modes of the crystal, the polarizabilities arising from A_1, E, and F_2 modes of the tetrahedra can be expressed as follows:

$$\alpha_{\rm cryst}^{A_1}(A_1)=\sqrt{2}\begin{pmatrix} 2a+\Delta_a & & \\ & 2a+\Delta_a & \\ & & 2a \end{pmatrix},\qquad \alpha_{\rm cryst}^{B_1}(A_1)=\sqrt{2}\begin{pmatrix} \Delta_a & & \\ & -\Delta_a & \\ & & 0 \end{pmatrix},$$

$$\alpha_{\rm cryst}^{A_1}(E(1))=\sqrt{2}\begin{pmatrix} -b & & \\ & -b & \\ & & 2b \end{pmatrix},\qquad \alpha_{\rm cryst}^{B_1}(E(1))=3\sqrt{2}\begin{pmatrix} -b & & \\ & b & \\ & & 0 \end{pmatrix},$$

Table 4. Frequencies of observed Raman lines (in cm^{-1}) of the low-frequency spectral range in $SrNi_2V_2O_8$ at a temperature 7 K. A symmetry assignment is based on the polarization selection rules

A_1(TO)	A_1(LO)	B_1+B_2	E(TO)
zz	$x'x'$	$x'x'$, $y'x'$	$x'z$
		78.5	81.7
		92.0	96.1
		131.2	115.2
		144.9	143.8
			148.6
			157.1
			159.9
164.3	165.3		
167.2	167.8		
		173.9	
		190.9	186.5
205.8		196.7	
229.9	230.2	230.4	
			232.3
			238.0
280.9	281.8		289.2
		298.9	
		304.2	
		314.3	316.1
334.5	334.9	322.7	
356.6	358.0		
370.5	368.4	374.0	
394.3	395.3		394.3
402.3	411.3		403.3
			417.2
		431.1	433.2
441.5	483.7	439.2	

$$\alpha^{A_1}_{\text{cryst}}\left(E(2)\right)=\sqrt{6}\begin{pmatrix} b & & \\ & b & \\ & & -2b \end{pmatrix}, \qquad \alpha^{B_1}_{\text{cryst}}\left(E(2)\right)=\sqrt{6}\begin{pmatrix} b & & \\ & -b & \\ & & 0 \end{pmatrix},$$

$$\alpha^{A_1}_{\text{cryst}}\left(F_2(x)\right)=\sqrt{2}\begin{pmatrix} \delta_c & & \\ & \delta_c & \\ & & -2\delta_c \end{pmatrix}, \qquad \alpha^{B_1}_{\text{cryst}}\left(F_2(x)\right)=\sqrt{2}\begin{pmatrix} -\delta_c & & \\ & \delta_c & \\ & & 0 \end{pmatrix},$$

$$\alpha^{B_2}_{\text{cryst}}\left(F_2(y)\right)=2\sqrt{2}\begin{pmatrix} & \delta_d & \\ \delta_d & & \\ & & \end{pmatrix}, \qquad \alpha^{B_2}_{\text{cryst}}\left(F_2(z)\right)=2\sqrt{2}\begin{pmatrix} & d & \\ d & & \\ & & \end{pmatrix}. \tag{4}$$

Here the upper indices mark irreps of the crystal modes while symbols in parentheses belong to the internal modes of tetrahedron.

Twice-degenerated modes of the crystal have *xz* and *yz* components of polarizability tensor only. That is why they can only originate from those modes of an individual molecule, whose polarizabilities contain such components. It follows from (3) that appreciable Raman intensity of twice degenerated modes in the crystal arises from the modes related to $E(2)$, $F_2(x)$, $F_2(y)$, and $F_2(z)$ molecular vibrations only. Theoretically these 4 degrees of freedom generate 8 crystal E modes, but only half of them possess nonzero Raman polarizability. In order to understand why this happens we can consider the example of $F_2(x)$ and $F_2(y)$ molecular degrees of freedom. These modes are dipolar that makes convenient their vector representation, as shown in Fig. 5. The *xz* components of crystal polarizability for modes shown in Fig. 5 are expressed as follows according to (4):

$$\alpha^{xz}_{\text{cryst}}(S_1)=\frac{1}{2\sqrt{2}}\left(\alpha_1^{yz}+\alpha_4^{yz}+\alpha_6^{yz}+\alpha_7^{yz}+\alpha_2^{xz}+\alpha_3^{xz}+\alpha_5^{xz}+\alpha_8^{xz}\right)=\sqrt{2}(c+d),$$

$$\alpha^{xz}_{\text{cryst}}(S_2)=\frac{1}{2\sqrt{2}}\left(\alpha_1^{yz}+\alpha_4^{yz}+\alpha_6^{yz}+\alpha_7^{yz}-\alpha_2^{xz}-\alpha_3^{xz}-\alpha_5^{xz}-\alpha_8^{xz}\right)=\sqrt{2}(c-d),$$

$$\alpha^{xz}_{\text{cryst}}(S_3)=\frac{1}{2\sqrt{2}}\left(\alpha_1^{yz}-\alpha_4^{yz}-\alpha_6^{yz}+\alpha_7^{yz}+\alpha_2^{xz}-\alpha_3^{xz}-\alpha_5^{xz}+\alpha_8^{xz}\right)=0,$$

$$\alpha^{xz}_{\text{cryst}}(S_4)=\frac{1}{2\sqrt{2}}\left(\alpha_1^{yz}-\alpha_4^{yz}-\alpha_6^{yz}+\alpha_7^{yz}-\alpha_2^{xz}+\alpha_3^{xz}+\alpha_5^{xz}-\alpha_8^{xz}\right)=0. \tag{5}$$

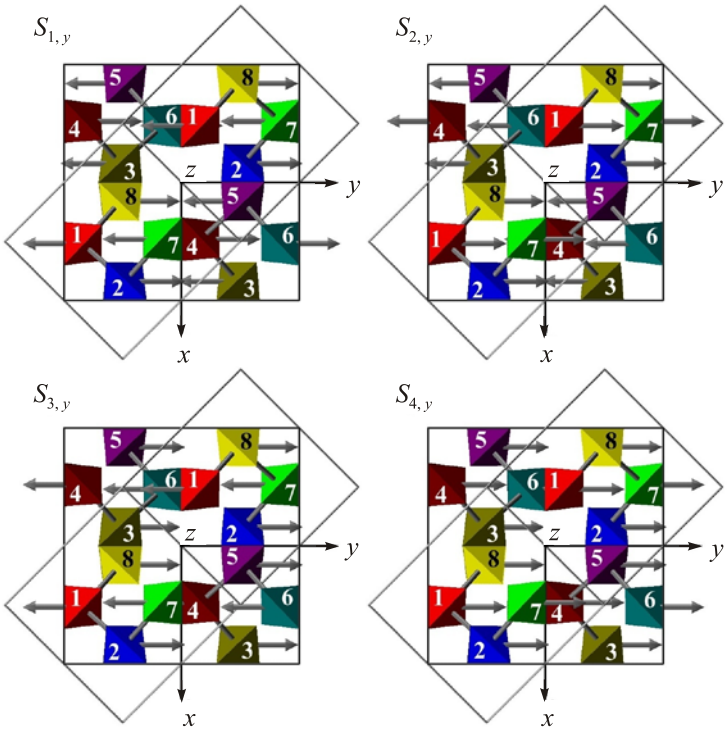

Fig. 5. (Color online) Patterns of *y* components of twice-degenerated modes in $SrNi_2V_2O_8$ originating from F_2 vibrational modes of tetrahedral $(VO_4)^{3-}$ complexes. Numeration of all tetrahedra belonging to primitive cell is used in expressions (5).

Modes S_3 and S_4 are silent due to orientation of one of the second order axes of the tetrahedra along crystallographic direction in the crystal basal plane. Mode S_2 is also weak because $c \approx d$. All nonzero polarizability tensors of the crystal for twice-degenerated modes are presented below:

$$\alpha^{E(x)}_{\text{cryst}}\left(E(2)\right) = 2\begin{pmatrix} & \delta_b & \\ \delta_b & & \\ & & \end{pmatrix}, \qquad \alpha^{E(y)}_{\text{cryst}}\left(E(2)\right) = 2\begin{pmatrix} & & \\ & \delta_b & \\ \delta_b & & \end{pmatrix},$$

$$\alpha^{E(x)}_{\text{cryst}}\left(F_2(z)\right) = 2\begin{pmatrix} & -\delta_d & \\ -\delta_d & & \\ & & \end{pmatrix}, \qquad \alpha^{E(y)}_{\text{cryst}}\left(F_2(z)\right) = 2\begin{pmatrix} & & \\ & -\delta_d & \\ -\delta_d & & \end{pmatrix},$$

$$\alpha^{E(x)}_{\text{cryst}}\left(F_2(x,y)\right) = \sqrt{2}\begin{pmatrix} & d+c & \\ d+c & & \\ & & \end{pmatrix}, \qquad \alpha^{E(y)}_{\text{cryst}}\left(F_2(x,y)\right) = \sqrt{2}\begin{pmatrix} & & \\ & d+c & \\ d+c & & \end{pmatrix},$$

$$\alpha^{E(x)}_{\text{cryst}}\left(F_2(x,y)\right) = \sqrt{2}\begin{pmatrix} & d-c & \\ d-c & & \\ & & \end{pmatrix}, \qquad \alpha^{E(y)}_{\text{cryst}}\left(F_2(x,y)\right) = \sqrt{2}\begin{pmatrix} & & \\ & d-c & \\ d-c & & \end{pmatrix}. \tag{6}$$

Results of the analysis are collected in Table 5.

With regard to $A_1(\nu_1)$ and $F_2(\nu_3)$ modes of high-frequency region, only one $A_1(\nu_1)$, one $B_2(\nu_3)$, and one $E(\nu_3)$ modes are expected to be intense if we assume that their polarizability is originated purely from the molecular polarizability. Taking into account small deviations from ideal form and orientation of the tetrahedra the weak $A_1(\nu_3)$, $B_1(\nu_1)$, $B_1(\nu_3)$, $B_2(\nu_3)$, and 2 $E(\nu_3)$ can be added. A comparison with experiment shows partial match. So, in E spectrum *one* intense and *three* weak lines are observed that differ from the prediction of *one* weak line. It is remarkable that in the frequency range of ν_1 mode no Raman signal of E polarization is detected, that is in agreement with the prediction. The analysis allows 4 $B_{1,2}$ modes

Table 5. Raman tensor components calculated for A_1, E and F_2 modes of tetrahedral $(VO_4)^{3-}$ complexes in $SrNi_2V_2O_8$ crystal. In the first column the symmetry of a free tetrahedron mode is indicated in parentheses

	xx	*yy*	*zz*
$A_1(A_1)$	$(2a+\Delta_a)\sqrt{2}$	$(2a+\Delta_a)\sqrt{2}$	$2a\sqrt{2}$
$A_1(F_2(x))$	$\delta_c\sqrt{2}$	$\delta_c\sqrt{2}$	$-2\delta_c\sqrt{2}$
$A_1(E(1))$	$-b\sqrt{2}$	$-b\sqrt{2}$	$2b\sqrt{2}$
$A_1(E(2))$	$b\sqrt{6}$	$b\sqrt{6}$	$-2b\sqrt{6}$
$B_1(A_1)$	$\Delta_a\sqrt{2}$	$-\Delta_a\sqrt{2}$	
$B_1(E(1))$	$-3b\sqrt{2}$	$3b\sqrt{2}$	
$B_1(E(2))$	$b\sqrt{6}$	$-b\sqrt{6}$	
$B_1(F_2(x))$	$-\delta_c\sqrt{2}$	$\delta_c\sqrt{2}$	
	xy=yx	*xz=zx*	*yz=zy*
$B_2(F_2(z))$	$2d\sqrt{2}$		
$B_2(F_2(y))$	$2\delta_d\sqrt{2}$		
$E(E(2))$		$2\delta_b$	$2\delta_b$
$E(F_2(x,y))$		$(d+c)\sqrt{2}$	$(d+c)\sqrt{2}$
$E(F_2(x,y))$		$(d-c)\sqrt{2}$	$(d-c)\sqrt{2}$
$E(F_2(z))$		$-2\delta_d$	$-2\delta_d$

with the most intense component in the frequency region of the ν_3 mode. Experimentally *two* intense and *four* weak lines are detected. One of the intense lines is close to the ν_1 frequency. It may mean that Δ_a term of the molecular polarizability is essential enough. In diagonal *zz* polarization (A_1 modes) there are *two* intense enough lines close to frequencies of ν_1 and ν_3 modes of free VO_4 tetrahedron. The analysis predicts less intense line due to δ_c term originated from the tetrahedra tilt. Its comparable with $A_1(\nu_1)$ mode intensity can not be explained in the proposed simple model where crystal polarizability is originated from the molecular polarizability only. Real situation may be too different from such a rough estimation. It means, for instance, that some of these internal modes of the molecular complexes may strongly polarize the crystal surrounding. Nevertheless the model provides evidence that a large number of $(VO_4)^{3-}$ complexes situated in the crystal structure may lead to the interferential quenching of their polarizability, resulting in a smaller number of intense lines observed in the Raman spectra indeed.

As for $E(\nu_2)$ and $F_2(\nu_4)$ modes of the tetrahedral $(VO_4)^{3-}$ complexes, the analysis predicts $3A_1+5B_{1,2}+4E$ lines in the Raman spectrum of the crystal, including those with small intensity. Remembering the group theory prediction for these modes, $5A_1+10B_{1,2}+10E$ (Table 1), we get about twice less detectable lines of this origin.

4.2. Modes related to Ni^{2+} *and* Sr^{2+} *degrees of freedom*

Sr^{2+} ions occupy positions with local symmetry C_2 in the crystal. Formally, $1A_1+1A_2+1B_1+1B_2+4E$ modes are caused by their degrees of freedom (Table 1). The coordination of every Sr^{2+} ion consists of 8 oxygens. It turned out that the surrounding ligands form approximately higher symmetry, than C_2 Wyckoff position for Sr^{2+}. The symmetry is close to C_{2v} with principal axis along *z* direction. Figure 6 clearly shows permissibility of that approximation.

Polarizability tensors connected with the motions of Sr^{2+} ions in their positions are the following:

$$\alpha_{z,1,2}(A_1)=\begin{pmatrix} a & & \\ & b & \\ & & c \end{pmatrix},\quad \alpha_{x,1,2}(B_1)=\begin{pmatrix} & & e \\ & & \\ e & & \end{pmatrix},\quad \alpha_{y,1,2}(B_2)=\begin{pmatrix} & & f \\ & & \\ f & & \end{pmatrix},$$

$$\alpha_{z,3,4}(A_1)=\begin{pmatrix} b & & \\ & a & \\ & & c \end{pmatrix},\quad \alpha_{x,3,4}(B_1)=\begin{pmatrix} & & f \\ & & \\ f & & \end{pmatrix},\quad \alpha_{y,3,4}(B_2)=\begin{pmatrix} & & e \\ & & \\ e & & \end{pmatrix}, \tag{7}$$

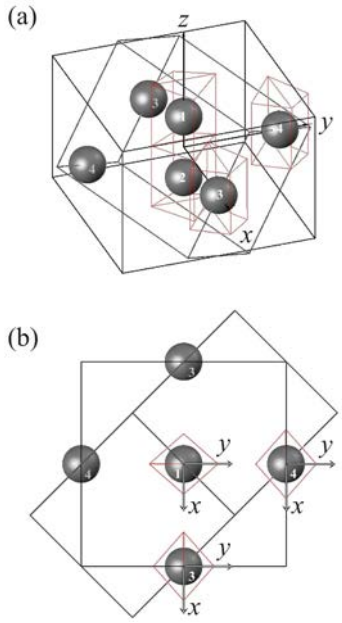

Fig. 6. (Color online) Structure of the Sr^{2+} coordination environment (a), and their projection on the basal plane (b) in $SrNi_2V_2O_8$ according to Refs. 20, 23. Atoms numeration and local coordinate systems are used in calculations.

The numeration follows Fig. 6. Symbols in parentheses relate to the C_{2v} point group irreps. Results of summations of expressions (7) through the normal modes originating from Sr^{2+} degrees of freedom in the crystal are presented in Table 6. As can be seen only $1A_1+1B_1+2E$ Sr^{2+} modes are expected to be intense in Raman. A deficit contains $1B_2+2E$ modes. Notably, tensors (7) do not contain *xy* components at all, so there are no sources to produce Raman intensity of B_2 mode. This is a consequence of the actual lack of rotation around the *z* axis of the oxygen polyhedron surrounding the Sr^{2+} ion.

Table 6. Raman tensor components calculated for Sr^{2+} and Ni^{2+} degrees of freedom in the $SrNi_2V_2O_8$ crystal. Labels *x*, *y*, *z* in the first column represent directions of the ions shifts

	xx	*yy*	*zz*
A_1, *z*	$(a+b)\sqrt{2}$	$(a+b)\sqrt{2}$	$c2\sqrt{2}$
B_1, *z*	$(a-b)\sqrt{2}$	$-(a-b)\sqrt{2}$	
	xy=yx	*xz=zx*	*yz=zy*
E, *x*		$(e+f)\sqrt{2}$	
E, *y*			$(e+f)\sqrt{2}$
E, *x*		$(e-f)\sqrt{2}$	
E, *y*			$(e-f)\sqrt{2}$

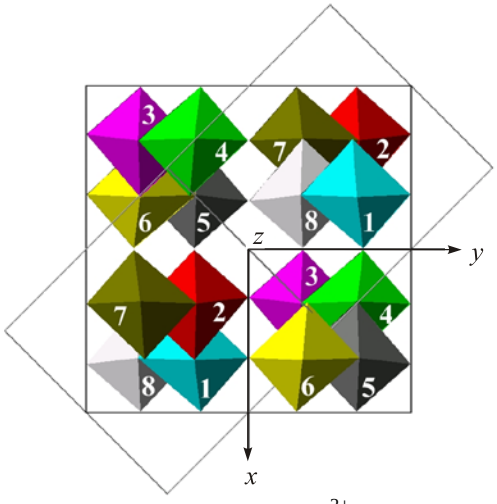

Fig. 7. (Color online) Structure of the Ni^{2+} coordination environment in $SrNi_2V_2O_8$ in the projection on basal plane according to Refs. 20, 23. Numeration of octahedrons is used in calculations.

Oxygen surroundings of Ni^{2+} in the structure of $SrNi_2V_2O_8$ looks like slightly distorted octahedron [20,23] as shown in Fig. 7. Similarly to Sr^{2+} we will describe the symmetry of the Ni^{2+} coordination environment as C_{2v} in the first approximation. *Eight* complexes are divided into *two* groups 1, 4, 6, 7 and 2, 3, 5, 8 which possess polarizability tensors analogous to (7). And the results are obtained in the same manner as for Sr^{2+} degrees of freedom. In spite of twice greater number of Ni^{2+} ions in the crystal structure, symmetry limitations in the described model do reduce effectively this number, so the expected number of intense Raman lines proves to be the same as for the case of Sr^{2+} ions (Table 6). Effective symmetry rise in this case leads to a bigger deficit of intense Raman lines. It contains for Ni^{2+} degrees of freedom $2A_1+2B_1+3B_2+4E$.

Summing up the total proposed deficit of Raman lines in the "lattice" frequency region, we obtain $4A_1+11B_{1,2}+12E$. This result is in a good agreement with experimental observations which estimate a lack of Raman lines in this region as $3A_1+15B_{1,2}+15E$. Notice, that the proposed analysis does not include exploration of the rotational and translational degrees of freedom of VO_4 tetrahedra which probably may produce extremely weak Raman signals too.

5. Summary

Vibrational Raman spectra of $SrNi_2V_2O_8$ are investigated in the 10–1000 cm^{-1} frequency range at various temperatures 7–300 K. There is no evidence of a structural phase transition in the investigated temperature range. Vibrational spectrum of the crystal naturally divides into two frequency ranges, namely "lattice" (50–500 cm^{-1}) and internal $\nu_{1,3}$ modes of $(VO_4)^{3-}$ tetrahedral complex (700–900 cm^{-1}). In the low-frequency range $11A_1+15B_{1,2}+16E$ modes are detected versus $14A_1+30B_{1,2}+31E$ allowed by the symmetry. In the high-frequency range there are $4A_1+6B_{1,2}+4E$ modes observed versus $4A_1+8B_{1,2}+8E$ allowed. A big deficit of the observed Raman lines is explained by a simple model which takes into account the higher symmetry of the complexes in the crystal structure than it is given by the position symmetry. Such "symmetrization" leads to interferential quenching of certain modes, which takes place due to big number of the identical molecules and ions in the $SrNi_2V_2O_8$ structure.

1. I. Affleck, *J. Phys.: Condens. Matter* **1**, 3047 (1989).
2. A. Smirnov and V. Glazkov, *J. Exp. Theor. Phys.* **105**, 861 (2007).
3. F.D.M. Haldane, *Phys. Rev. Lett.* **50**, 1153 (1983)
4. F.D.M. Haldane, *Phys. Lett. A* **93**, 464 (1983).
5. M. Takahashi, *Phys. Rev. Lett.* **62**, 2313 (1989).
6. O. Golinelli, T. Jolicoeur, and R. Lacaze, *J. Phys.: Condens. Matter* **5**, 1399 (1993).
7. S.R. White and I. Affleck, *Phys. Rev. B* **77**, 134437 (2008).
8. S. Ma, C. Broholm, D.H. Reich, B.J. Sternlieb, and R.W. Erwin, *Phys. Rev. Lett.* **69**, 3571 (1992).
9. G. Xu, G. Aeppli, M.E. Bisher, C. Broholm, J.F. DiTusa, C.D. Frost, T. Ito, K. Oka, R.L. Paul, 10. H. Takagi, and M.M.J. Treacy, *Science* **289**, 419 (2000).
10. P. Lemmens, G. Güntherodt, and C. Gros, *Phys. Rep.* **375**, 1 (2003).
11. P.E. Sulewski and S.-W. Cheong, *Phys. Rev. B* **51**, 3021 (1995).
12. T. Sakai and M. Takahashi, *Phys. Rev. B* **42**, 4537 (1990).
13. A. Zheludev, T. Masuda, I. Tsukada, Y. Uchiyama, K. Uchinokura, P. Böni, and S.-H. Lee, *Phys. Rev. B* **62**, 8921 (2000).
14. A. Zheludev, T.Masuda, K. Uchinokura, and S.E. Nagler, *Phys. Rev. B* **64**, 134415 (2001).
15. Y. Uchiyama, Y. Sasago, I. Tsukada, K. Uchinokura, A. Zheludev, T. Hayashi, N. Miura, and P. Böni, *Phys. Rev. Lett.* **83**, 632 (1999).
16. A.K. Bera and S.M. Yusuf, *Phys. Rev. B* **86**, 024408 (2012).
17. B. Pahari, K. Ghoshray, R. Sarkar, B. Bandyopadhyay, and A. Ghoshray, *Phys. Rev. B* **73**, 012407 (2006).
18. Z. He and Y. Ueda, *J. Phys. Soc. Jpn.* **77**, 013703 (2008).
19. A.K. Bera, B. Lake, A.T.M.N. Islam, B. Klemke, E. Faulhaber, and J.M. Law, *Phys. Rev. B* **87**, 224423 (2013).
20. A.K. Bera, B. Lake, A.T.M.N. Islam, O. Janson, H. Rosner, A. Schneidewind, J.T. Park, E. Wheeler, and S. Zander, *Phys. Rev. B* **91**, 144414 (2015).
21. A.K. Bera, B. Lake, A.T.M.N. Islam, and A. Schneidewind, *Phys. Rev. B* **92**, 060412R (2015).
22. Z. Wang, M. Schmidt, A.K. Bera, A.T.M.N. Islam, B. Lake, A. Loidl, and J. Deisenhofer, *Phys. Rev. B* **87**, 104405 (2013).
23. R. Wichmann and H. Müller-Buschbaum, *Rev. Chim. Miner.* **23**, 1 (1986).
24. N. Weinstock, H. Schulze, and A. Müller, *J. Chem. Phys.* **59**, 5063 (1973).
25. E. Anachkova, M. Gospodinov, P. Svestarov, T. Milenov, A. Nikolov, V. Tasev, Y. Markov, M. Limonov, G. Bruchman, *J. Mol. Struct.* **219**, 31 (1990).

26. J.D. Pless, H.-S. Kim, J.P. Smit, X. Wang, P.C. Stair, and K.R. Poeppelmeier, *Inorg. Chem.* **45**, 514 (2006).
27. R.L. Frost, S.J. Palmer, J. Čejka, J. Sejkora, J. Plášil, S. Bahfenne, and E.C. Keeffe, *J. Raman Spectrosc.* **42**, 1701 (2011).
28. N. Zhang, J. Wang, X. Hu, H. Zhang, C.C. Santos, A.P. Ayala, and I. Guedes, *J. Solid State Chem.* **184**, 905 (2011).
29. V. Panchal, S. López-Moreno, D. Santamaría-Pérez, D. Errandonea, F.J. Manjón, P. Rodríguez-Hernandez, A. Muñoz, S.N. Achary, and A.K. Tyagi, *Phys. Rev. B* **84**, 024111 (2011).
30. L. Rghioui, L. Benarafa, J. El Jastimi, A. El Hajji, A. Lorriaux, and F. Wallart, *J. Mater. Environ. Sci.* **3** (1), 58 (2012).
31. W.P. Griffith and T.D. Wickins, *J. Chem. Soc.* (A): *Inorg. Phys. Theor.* 1087 (1966).
32. R.D. Shannon, *Acta Cryst. A* **32**, 751 (1976).
33. A. de Andres, J.L. Martinez, R. Saez-Puche, and A. Salinas-Sanchez, *Solid State Commun.* **82**, 931 (1992).
34. G. Gou, I. Grinberg, A.M. Rappe, and J.M. Rondinelli, *Phys. Rev. B* **84**, 144101 (2011).
35. C.M. Julien, A. Mauger, K. Zaghib, R. Veillette, and H. Groult, *Ionics* **18**, 625 (2012).
36. V. Gnezdilov, V. Kurnosov, P. Lemmens, Yu. Pashkevich, A.K. Bera, A.T.M.N. Islam, and B. Lake, Magnetic Excitations in the Symmetry Protected Topological Quasi-One-Dimensional Haldane Phase of $SrNi_2V_2O_8$, to be published.